

Chapter 2

The SD Oscillator

This chapter introduces briefly the smooth and discontinuous (SD) oscillator which is a simple mechanical model or a geometrical oscillator with both smooth and discontinuous dynamics depending on the value of the geometrical parameter. Like the traditional harmonic oscillator, this model is also a simple mass-spring system comprising a lumped mass linked by a pair of linear springs pinned to its rigid supports vibrating along the perpendicular bisector of the supports. The overview of the system with the definitions and the fundamental properties are given here without detailed explanation, and will be expanded and discussed in the following chapters from Chaps. 3 to 6.¹

2.1 Introduction

As mentioned in the introduction, Chap. 1, in addition to the smooth systems like Duffing oscillator, Lorenz system and van de Pol oscillator as well, many examples arise from mechanical and civil engineering [1, 2], electronics [3, 4], control [5, 6], computer graphics [7, 8], biology [9, 10], and others, which are non-smooth or discontinuous. This oscillator is motivated by the growing interest in the system which is not valid for the conventional nonlinear dynamics, especially. Although some theoretical foundations have been laid in the work by Filippov [11], Feigin [12], Kunze [13], Peterka [14], Shaw and Holmes [15] and Nordmark [16], there is a large disparity between development and understanding of smooth and discontinuous (non-smooth) systems.

¹This part of this chapter involves a common work by the authors with Professors Celso Grebogi, Ekaterina Pavlovskaja, J. Michael Thompson, Center for Applied Dynamics Research, Aberdeen University, King's College, Aberdeen AB24 3UE, Scotland, UK.

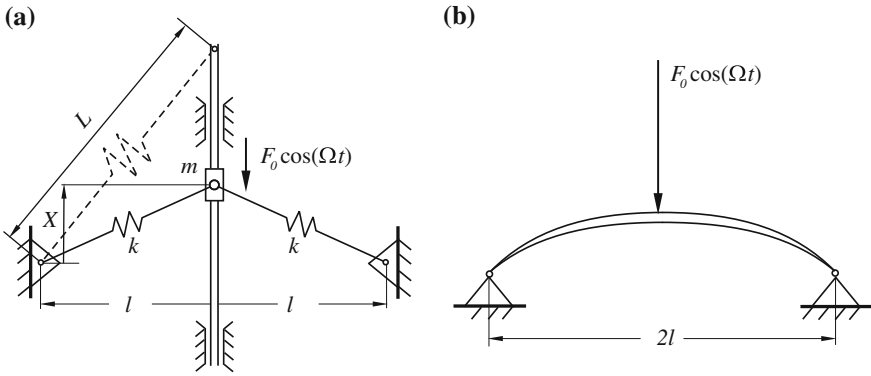


Fig. 2.1 a A mechanical oscillator consisting of a lumped mass m linked by a pair of linear springs with stiffness k and the equilibrium length L pinned to rigid supports abstracted from the first mode of a simple elastic arch demonstrated in **b**

An archetypal oscillator whose nonlinearity can be smooth or discontinuous depending on the value of the smoothness parameter α is proposed and studied. As the considered oscillator has properties of both a smooth and a discontinuous system (at the limit), potentially a wealth of knowledge can be drawn from the well developed theory of continuous dynamics. Physically (as shown in Fig. 2.1a) this oscillator is similar to a snap-through truss system. It comprises a mass, m , linked by a pair of inclined elastic springs which are capable of resisting both tension and compression; each spring of stiffness k is pinned to a rigid support. This model is inspired on the elastic arch described by Thompson and Hunt in [17] (see Fig. 2.1b). Although the springs themselves provide linear restoring resistance, the resulting vertical force on the mass is strongly nonlinear because of changes to the geometric configuration. Although the springs are linear, the system behaves a strongly nonlinearity due to the geometrical configuration. In the smooth regime, the system bears significant similarities to the Duffing oscillator, exhibiting the standard dynamics of hyperbolic structure patterns associated with equilibrium bifurcation of a supercritical pitchfork. The dynamics might be transformed from a single-well into a double-well behaviour at the degenerate value of the geometrical parameter. In the discontinuous case however, there is a substantial departure in the dynamics from the standard one. The system behaves a nonstandard dynamics caused by the loss of local hyperbolicity due to the collapse of the stable and unstable manifolds of the stationary state. In the presence of damping and external excitation, the system bears co-existence of attractors and a chaotic saddle, which becomes a chaotic attractor when the smoothness parameter drops to zero. This attractor may bifurcate to a large period periodic attractor or to a chaotic sea with islands of quasi-periodic attractors depending on the amplitude of the damping. All along this book the oscillator will be referred to as the SD oscillator and the attractors indicates the SD attractors.

2.2 Unperturbed Oscillator

The mechanical model of a mass-spring system dealt with all along the present book is very simple, which is inspired by the first mode of an elastic arch described in [17, 18], seen in Fig. 2.1b, and is similar to a snap-through truss system. As shown in Fig. 2.1a, it is constructed with a lumped mass m linked by a pair of linearly elastic springs with stiffness k and the equilibrium length L being capable of resisting both in tension and in compression pinned to a rigid frame. Although the springs themselves provide a linear restoring resistance, the resulting vertical force supplied to the mass is nonlinear because of the geometrical configuration, which is exactly a model for large deformations of the arch in Fig. 2.1b.

The equation of the motion of mass m is obtained according to the geometrical configuration of the springs, due to the Pythagorean theorem [19], and the Hooke's Law [20, 21].

$$m\ddot{X} + 2kX \left(1 - \frac{L}{\sqrt{X^2 + l^2}} \right) = 0, \quad (2.1)$$

where L is the natural length of each spring, X is the displacement of the mass and l is the half distance between the rigid supports. System (2.1) can be made dimensionless by letting $\omega_0^2 = \frac{2k}{m}$, $x = \frac{X}{L}$ and $\alpha = \frac{l}{L} \geq 0$,

$$\ddot{x} + \omega_0^2 x \left(1 - \frac{1}{\sqrt{x^2 + \alpha^2}} \right) = 0, \quad (2.2)$$

where α stands for a smooth geometrical parameter, which defines the geometry of the oscillator as shown in Fig. 2.1a with its full physical practice. From the mechanical point of view, for $\alpha > 0$ the system represents a pre-stressed discrete elastic string presenting an archetypal smooth oscillator. If $\alpha = 0$, the model corresponds to an oscillating mass supported by two parallel vertical springs, as shown in Fig. 3.1a. It is worth reiterating here that the discontinuous dynamics can be obtained by decreasing of the smoothness parameter $\alpha \rightarrow 0$. Equation (2.2) is now written as the following.

$$\ddot{x} + \omega_0^2 (x - \text{Sign}(x)) = 0, \quad (2.3)$$

where $\text{Sign}(x)$ is the sign of x . System (2.3) is the limit case of system (2.2) when $\alpha = 0$ building up an archetypal discontinuous oscillator consisting a pair of opposite directed harmonic oscillators. Usually system (2.2) and (2.3) is called the SD oscillator throughout the book: S means smooth and D refers to discontinuous.

It is addressed that even the equation of motion (2.2) is derived by the simple Hooke's Law which is also the simple harmonic oscillator [21], the resistance of our model is nonlinear depending on the geometrical configuration, which can be regarded as the generalized Hooke's Law with the stiffness might be positive, negative or zero (quasi-zero) depending on the geometrical configuration of the system.

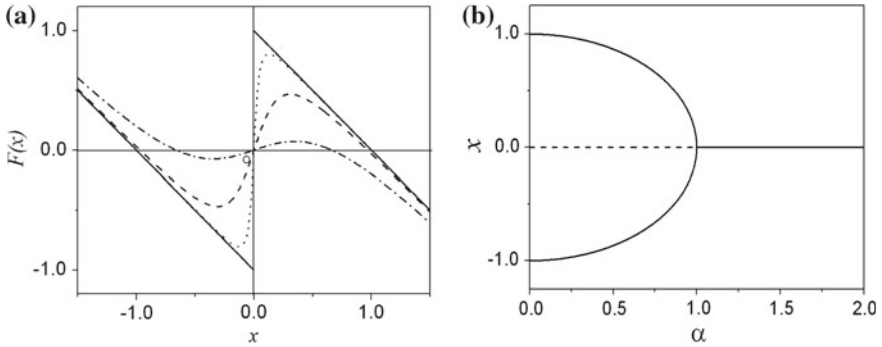


Fig. 2.2 **a** Nonlinear restoring force, $F(x)$; *solid line* marks the discontinuous case for $\alpha = 0$, *dotted*, *dash-dotted* and *dashed curves* are the smooth cases for $\alpha = 0.1, 0.5$ and $\alpha = 0.75$, respectively, and **b** The equilibrium bifurcation: the *solid line* marks the stable and the *dashed* indicates the unstable branches with bifurcation point at $\alpha = 1$

The restoring force reads $F(x) = -\omega_0^2 x \left(1 - \frac{1}{\sqrt{x^2 + \alpha^2}} \right)$ is plotted for $\omega_0 = 1$ in Fig. 2.2a for different values of parameter α . The solid line represents the discontinuous case $\alpha = 0$, the dotted, the dashed dotted and the dashed lines mark the smooth cases, for $\alpha = 0.01, 0.5,$ and 0.75 respectively.

To examine the influence of parameter α on the dynamics of (2.2) we construct the bifurcation diagram, depicted in Fig. 2.2b. The system undergoes a supercritical pitchfork bifurcation at $\alpha = 1$ where the stable branch $x = 0, \alpha \geq 1$ bifurcates into two stable branches at $x = \pm\sqrt{1-\alpha^2}, 0 \leq \alpha < 1$, while the state branch $x = 0$ is now becomes unstable. The Hamiltonian for system (2.2) can be written as

$$H(x, y) = \frac{1}{2}y^2 + \frac{1}{2}\omega_0^2 x^2 - \omega_0^2 \sqrt{x^2 + \alpha^2} + \omega_0^2 \alpha, \quad (2.4)$$

where $\dot{x} = y$. With the help of the Hamiltonian function (2.4), the trajectories can be classified and analyzed. For both continuous and discontinuous cases, the phase portraits of systems (2.2) or (2.4) are plotted for different values of the Hamiltonian $H(x, y) = E$. For instance, for the smooth nonlinearity, $\alpha = 0.5$, the dynamical behaviour of double-well is similar to that of the Duffing oscillator [22], shown in Fig. 2.3a. For $\alpha = 0$, the behaviour is singular, as shown in Fig. 2.3b: the orbits for $E > 0$ are composed of two large segments of circles with their centers located at $(-1, 0)$ and $(1, 0)$ connected at $x = 0$. The case of $E < 0$ is represented by two families of circles. It is very interesting that the level $E = 0$ for the discontinuous system (2.3) is made up of two circles centered at $(\pm 1, 0)$ connecting at the singular point $(0, 0)$, which form a special singular homoclinic-like orbits. Even system (2.3) is discontinuous at $(0, 0)$ without eigenvalues and eigenvectors., the structure around it indicates a saddle-like behaviour, which is named the saddle-like equilibrium. The loss of hyperbolicity at $(0, 0)$ is caused by the tangency of the stable and unstable eigen directions. The pair of circles excluding the point $(0, 0)$ are not the manifolds of the singularity, but the flow along these circles approaches the point as $x \rightarrow 0$,

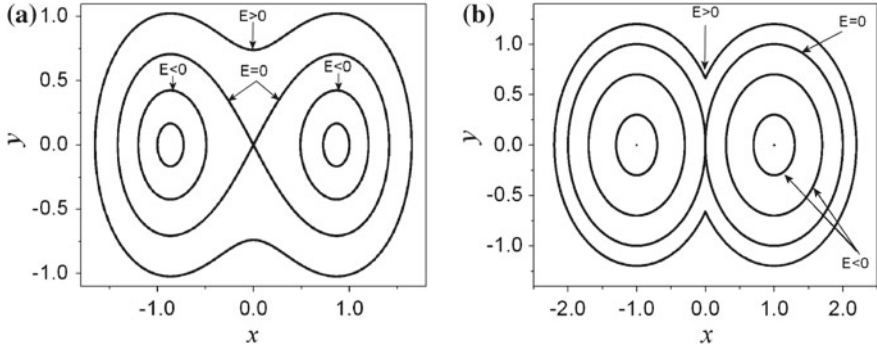


Fig. 2.3 Phase portraits; **a** smooth case for $\alpha = 0.5$ and **b** discontinuous case for $\alpha = 0$

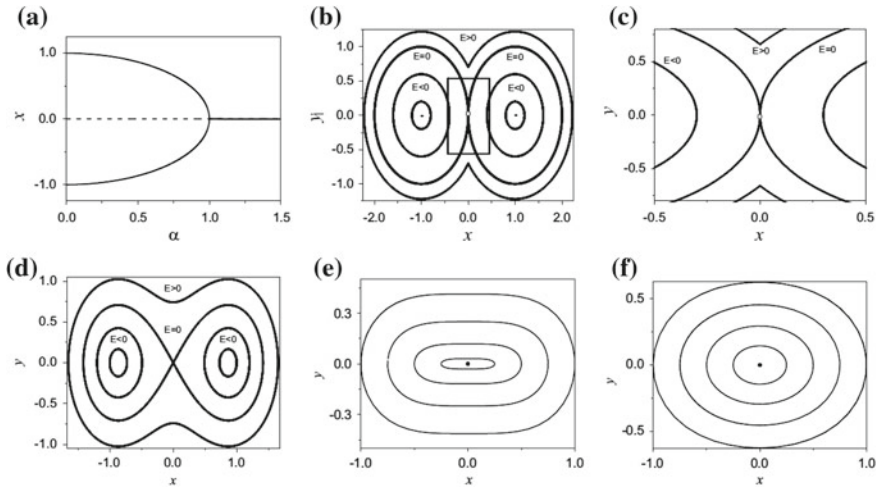


Fig. 2.4 **a** Equilibrium bifurcation and the Phase portraits of the SD oscillator: **b** phase portrait for $\alpha = 0$ with a homoclinic-like orbit composing a pair of cycles connected at a saddle-like singularity, the box area, **c** locally amplified structure, and **d** the portraits for double-well behaviour when $0 < \alpha < 1$ and **f** the single-well characteristic when $\alpha > 1$ transformed at the degenerate case **e** when $\alpha = 1$

and it will be trapped by the singularity. The solution of the special homoclinic-like orbits can be formulated as

$$\Gamma = \{(x_{\pm}(t), y_{\pm}(t)), t \in (-\frac{\pi}{\omega_0}, \frac{\pi}{\omega_0})\} \cup \{(0, 0)\}, \quad (2.5)$$

where $(x_{\pm}(t), y_{\pm}(t)) = (\pm 1 \pm \cos \omega_0 t, \mp \sin \omega_0 t)$.

Here system (2.2) together with the limit case of system (2.3) is named the **SD oscillator**, S means the smooth and D indicates discontinuous, respectively.

Figure 2.4 summaries all the patterns of the unperturbed dynamics of the SD oscillator for the equilibrium bifurcations with the supercritical pitchfork in Fig. 2.4a and the corresponding phase portraits as the geometrical parameter α varies. For

$\alpha > 0$ the system admits the standard smooth dynamics transforming the single-well dynamics from $\alpha > 1$, shown in Fig. 2.4f, into double-well behaviour to $0 < \alpha < 1$, shown in Fig. 2.4d, which results in the so-called single stability and bistability shifting at $\alpha = 1$ with degenerate singularity, shown in Fig. 2.4e, which will be investigated in the following chapters. As the geometrical parameter α decreases to $\alpha = 0$, a sudden change happens leading to a nonstandard dynamics, as shown in Fig. 2.4b and the local amplified boxed area in Fig. 2.4c, which is caused by the loss of local hyperbolicity due to the collapse of the eigen direction of the stable and unstable manifolds at the stationary state. This discontinuous behaviour results in the homoclinic-like orbit consisting of a pair of cycles connected at the saddle-like equilibrium $(0, 0)$ centered at $(\pm 1, 0)$ respectively.

2.3 The Transition from Smooth to Discontinuous Dynamics

Now suppose system (2.1) is perturbed by a viscous damping and an external harmonic excitation of amplitude F_0 and frequency Ω . This leads to the following perturbed system,

$$m\ddot{X} + \delta\dot{X} + 2kX\left(1 - \frac{L}{\sqrt{X^2 + l^2}}\right) = F_0 \cos \Omega t. \quad (2.6)$$

Again system (2.6) can be written in a dimensionless form by letting $\tau = \omega_0 t$, $f_0 = \frac{F_0}{2kL}$, $\xi = \frac{\delta}{2m\omega_0}$ and $\omega = \frac{\Omega}{\omega_0}$,

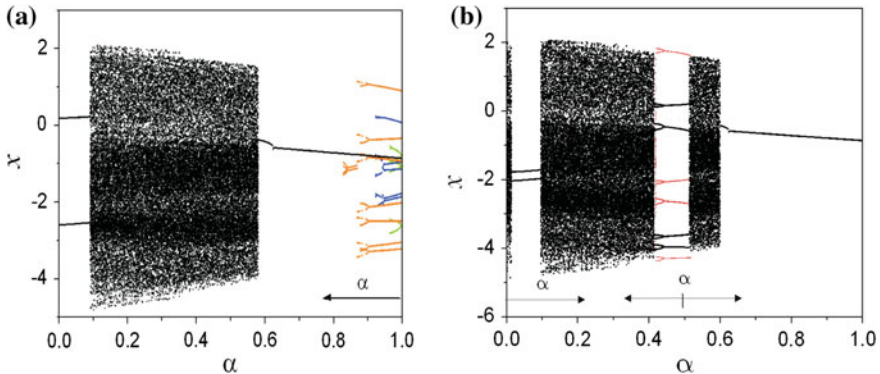


Fig. 2.5 Bifurcation diagrams for x versus α constructed for: **a** Decreasing from $\alpha = 1$ and following the attractors starting with period 1 (black), period 3 (green), 5 (blue) and 7 (red) respectively, **b** first, increasing from $\alpha = 0$ to 0.3 following the attractor starting with the initial condition $(1,0)$. Second, decreasing α from 0.5 to 0.3 and increasing from α from 0.5 to 1, following the attractors starting with two period 4 solutions respectively

$$x'' + 2\xi x' + x(1 - \frac{1}{\sqrt{x^2 + \alpha^2}}) = f_0 \cos \omega \tau, \tag{2.7}$$

where “'” denotes the differentiation with respect to τ .

Numerical simulations have been carried out by using Runge–Kutta method for system (2.7) for only the smooth case for $\alpha > 0$, while in the discontinuous case for $\alpha = 0$ the analytical technique is developed, the details will be given in the following chapters. It is always assumed $f_0 = 0.8$, $\xi = 0.01\sqrt{2}$ and $\omega = 0.75\sqrt{2}$ in the following calculations. Figure 2.5 shows bifurcation diagrams constructed for x sampled stroboscopically at phase zero versus control parameter α as α decreases from 1 to 0 (Fig. 2.5a) and α increases from 0 to 0.3 and from 0.5 to 1 and decreases from 0.5 to 0.3 (Fig. 2.5b). The system has co-existing periodic attractors and a strange chaotic attractor for $\alpha > 0$. However, for $\alpha = 0$ the system exhibits chaotic and periodic solutions with unusual high periods. These behaviours can be controlled by

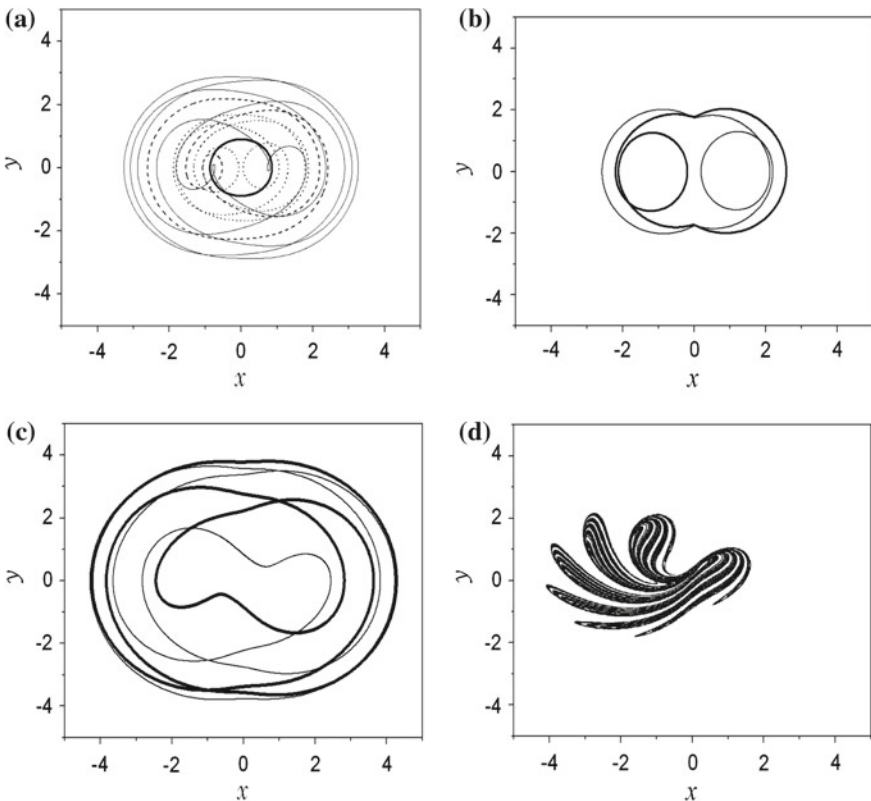


Fig. 2.6 Co-existence of periodic motions: **a** Period 1 (*thick line*), period 3 (*dash line*), 5 (*dotted line*) and 7 (*thin line*) respectively for $\alpha = 1.0$, **b** a pair of period two solutions for $\alpha = 0.05$, **c** and **d** represent the pair of period four and the chaotic attractor for $\alpha = 0.5$ with the largest Lyapunov exponent 0.1065

the strength of the damping. The main feature of these attractors is their topological similarity since they are associated with the hyperbolic stationary state. This similarity also holds for $\alpha > 0$. The chaotic attractor can become a chaotic sea with islands representing quasi periodic behaviour for $\alpha = 0$ and $\xi = 0$.

Figure 2.5a also shows the co-existing periodic solution of period one, three, five and seven at $\alpha = 1$ (orbits are shown in Fig. 2.6a) and their bifurcations under decreasing α . Other co-existing periodic solutions are found for $\alpha \in (0, 0.1)$, as shown in Fig. 2.5a, b. These two co-existing period 2 solutions are symmetrical and the orbits for $\alpha = 0.05$ are presented in Fig. 2.6b. For $\alpha \in (0.41, 0.52)$ a chaotic attractor co-exists with two period 4 solutions and the corresponding trajectories and the chaotic attractor are shown in Fig. 2.6c, d, respectively.

In addition to the co-existence of different attractors, the system exhibits chaotic transient behaviour characterized by chaotic saddles, see [23–25]. The transient and the final periodic attractor are shown in Fig. 2.7b, c for $\alpha = 0.01$ and $\alpha = 0.001$

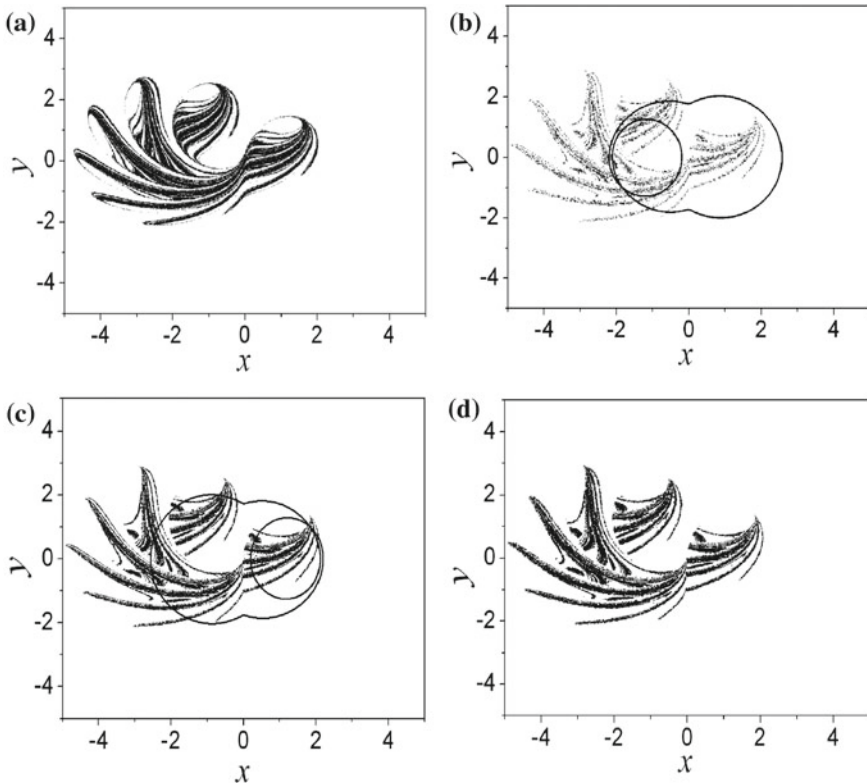


Fig. 2.7 **a** Chaotic attractor for $\alpha = 0.1$ with the largest Lyapunov exponent 0.0812, **b** chaotic saddle leading to period 2 solution for $\alpha = 0.01$ and **c** chaotic saddle leading to period 2 solution for $\alpha = 0.001$ **d** chaos for $\alpha = 0$ with the largest Lyapunov exponent 0.0480

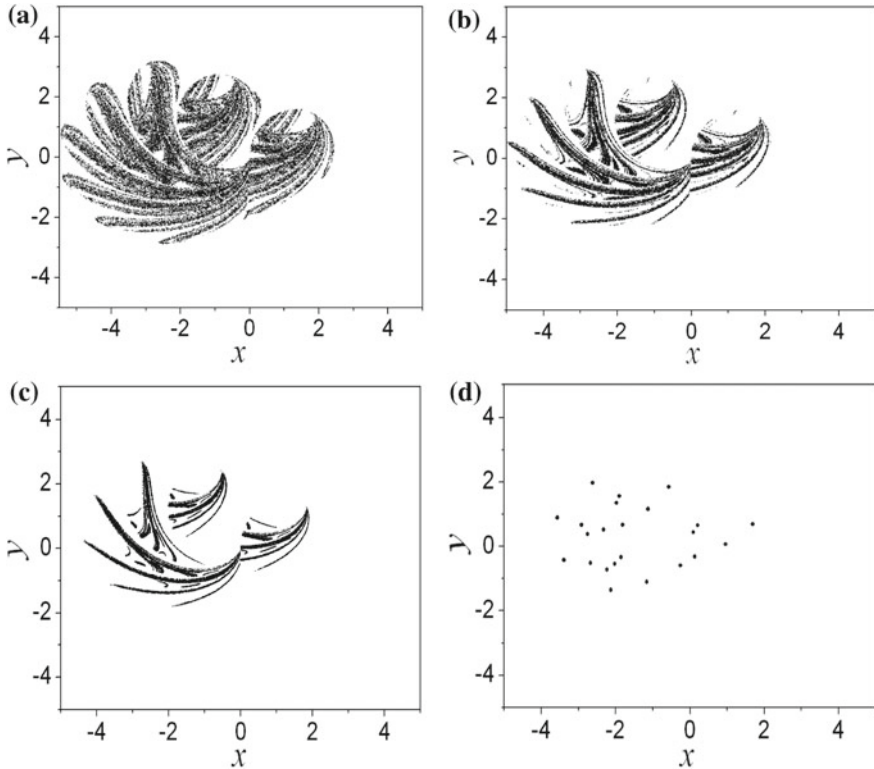
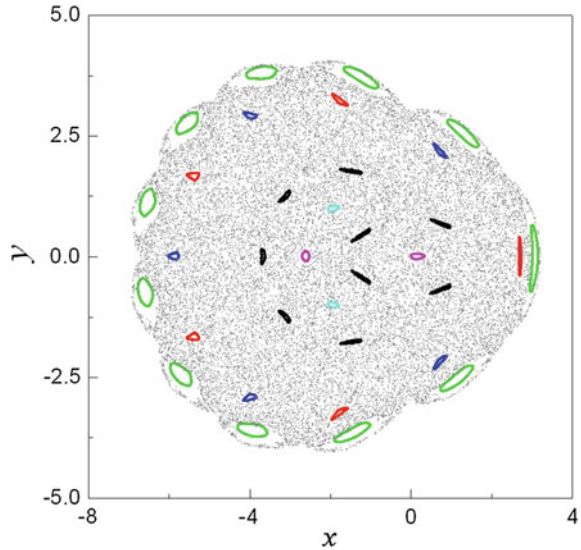


Fig. 2.8 Poincaré sections for $f_0 = 0.8$, $\omega = 0.75\sqrt{2}$, $\alpha = 0$; **a** chaotic attractor for $\xi = 0.005$ with the largest Lyapunov exponent 0.0525, **b** chaotic motion for $\xi = 0.0125$ with the largest Lyapunov exponent 0.0505, **c** chaotic motion for $\xi = 0.025$ with the largest Lyapunov exponent 0.0470 and **d** high periodic motion of period 23 for $\xi = 0.028$

respectively. The set of Poincaré maps shown in Fig. 2.7 for $\alpha = 0.1, 0.01, 0.001$ and 0 shows the topological similarity now associated with the discontinuity at the origin. The co-existing period 2 solutions persist for $\alpha = 0$ and the chaotic saddle becomes a chaotic attractor for $\alpha = 0$ as shown in Fig. 2.7d. The behaviour of this chaotic attractor can be controlled by the damping ratio ξ . Other attractors are presented in Fig. 2.8a for $\xi = 0.005$, Fig. 2.8b for $\xi = 0.0125$ and Fig. 2.8c for $\xi = 0.025$. A high period periodic attractor is shown in Fig. 2.8d having period 23 for $\xi = 0.028$. For both $\alpha = 0$ and $\xi = 0$, a chaotic sea and quasi-periodic behaviour can also be inferred via a semi-analytical method, see [26]. Figure 2.9 shows the chaotic sea together with a pair of quasi-period 2 solutions, a pair of quasi-period 5 solutions, the quasi-period 9 and the quasi-period 11 solutions respectively. The largest Lyapunov exponent for all the chaotic attractors presented here have been calculated using the chaos synchronization method, see [27] for instance, as shown in the captions for the corresponding figures.

Fig. 2.9 Poincaré section for $f_0 = 0.8$, $\omega = 0.75\sqrt{2}$, $\alpha = 0$: chaotic sea or stochastic web and quasi-periodic trajectories (islands) for $\xi = 0$



Even only the primary characteristics of the perturbed oscillator are presented in this section, the main features of the system show that decreasing α further creates chaotic transients around a chaotic saddle, which leads to periodic orbits as the time increases. This chaotic transient becomes a chaotic attractor for $\alpha = 0$. The attractor can deform in shape or bifurcate to a high period periodic attractor depending on the strength of damping, or even can become a chaotic sea or stochastic web with islands of quasi-periodic trajectories for $\xi = 0$. It is also interesting to compare the finger like topology of the chaotic attractors found here with that observed by Thompson et al. in [28, 29]. The attractors shown in this chapter (2.2) and (2.3) are called the SD attractors: attractors of system (2.7) for both smooth ($\alpha > 0$) and discontinuous stage ($\alpha = 0$).

2.4 Summary

Let us close this chapter by a brief survey to list the main features that arise from this archetypal SD oscillator. At the first point, one must keep in mind that the unperturbed smooth oscillator has a double-well characteristics for $0 < \alpha < 1$, which is similar to Duffing oscillator and the system can be consequently integrated using classical methods for smooth systems such as Runge–Kutta method. However, it is different from the Duffing oscillator since there is no analytical solutions depending upon the elliptic functions. Furthermore, in the limit case of the SD oscillator, that is the discontinuous oscillator, classical methods no longer apply. This global qualitative analysis being presented, the following chapters we will study everything in detail,

coming back to the basic mathematical tools when they are necessary or simply for the book to be self-contained.

References

1. Woo, K. C., Pavlovskaja, E., Wiercigroch, M., & Rodger, A. A. (2003). Modelling of ground moling dynamics by an impact oscillator with a frictional slider. *Meccanica*, 38(1), 85–97.
2. Karpenko, E. V., Pavlovskaja, E., & Wiercigroch, M. (2004). Nonlinear dynamic interactions of a jeffcott rotor with a preloaded snubber ring. *Journal of Sound and Vibration*, 276(1–2), 361–379.
3. Banerjee, S., & Chakrabarty, K. (1998). Nonlinear modeling and bifurcations in the boost converter. *IEEE Transactions on Power Electronics*, 13(2), 252–260.
4. Banerjee, S., Ott, E., Yorke, J. A., & Yuan, G. H. (1997). Anomalous bifurcations in dc-dc converters: borderline collisions in piecewise smooth maps. In *28th annual IEEE power electronics specialists' conference, PESC '97 record*, (Vol. 2), 22–27 Jun 1997, St. Louis, MO, pp. 1337–1344. IEEE.
5. Slotine, J. J., & Sastry, S. S. (1983). Tracking control of non-linear systems using sliding surfaces with application to robot manipulators. *International Journal of Control*, 38(2), 465–492.
6. Richard, P. Y., Cormerais, H., & Buisson, J. (2006). A generic design methodology for sliding mode control of switched systems. *Nonlinear Analysis, Theory, Methods and Applications*, 65(9), 1751–1772.
7. Luo, A. C. J., & Burkhart, H. (1995). Intensity-based cooperative bidirectional stereo matching with simultaneous detection of discontinuities and occlusions. *International Journal of Computer Vision*, 15(3), 171–188.
8. Nishita, T., Sederberg, T. W., & Kakimoto, M. (1990). Ray tracing trimmed rational surface patches. *Computer Graphics*, 24(4), 337–345.
9. Kribs-Zaleta, C. M. (2004). To switch or taper off: The dynamics of saturation. *Mathematical Biosciences*, 192(2), 137–152.
10. Drulhe, S., Ferrari-Trecate, G., De Jong, H., & Viari, A. (2006). Reconstruction of switching thresholds in piecewise-affine models of genetic regulatory networks. In J. P. Hespanha & A. Tiwari (Eds.), *Hybrid systems: computation and control* (Vol. 3927, pp. 184–199)., Lecture notes in computer science Heidelberg: Springer.
11. Filippov, A. F. (1988). *Differential equations with discontinuous right-hand sides: Control systems* (Vol. 18)., Mathematics and its applications The Netherlands: Springer. Originally published in Russian.
12. Feigin, M. I. (1966). Resonance behaviour of a dynamical system with collisions. *Journal of Applied Mathematics and Mechanics*, 30(5), 1118–1123.
13. Kunze, M. (2000). *Non-smooth dynamical systems*. Berlin: Springer.
14. Peterka, F. (1981). *Introduction to vibration of mechanical systems with internal impacts*. Prague: Academia.
15. Shaw, S. W., & Holmes, P. J. (1983). A periodically forced piecewise linear oscillator. *Journal of Sound and Vibration*, 90(1), 129–155.
16. Nordmark, A. B. (1991). Non-periodic motion caused by grazing incidence in an impact oscillator. *Journal of Sound and Vibration*, 145(2), 279–297.
17. Thompson, J. M. T., & Hunt, G. W. (1973). *A general theory of elastic stability*. London: Wiley.
18. Savi, M. A., & Pacheco, P. M. C. L. (2003). Transient chaos in an elasto-plastic beam with hardening. *Journal of Brazilian Society of Mechanical Sciences and Engineering*, 25(2), 189–193.
19. Maor, E. (2007). *The Pythagorean theorem: A 4,000-year history*. Princeton: Princeton University Press.

20. Drake, E. T. (1996). *Restless Genius: Robert Hooke and his earthly thoughts*. Oxford: Oxford University Press.
21. Lewin, W. (1999). *Hooke's Law, simple harmonic oscillator.*, MIT course 8.01: Classical mechanics, lecture 10. (ogg) (videotape) Cambridge: MIT OCW.
22. Guckenheimer, J., & Holmes, P. (1983). *Nonlinear oscillation, dynamical system and bifurcation of vector fields*. New York: Springer.
23. Lai, Y. C., & Lerner, D. (1998). Effective scaling regime for computing the correlation dimension from chaotic time series. *Physica D-Nonlinear Phenomena*, 115, 1–18.
24. Tel, T. (1986). Characteristic exponents of chaotic repellers as eigenvalues. *Physics Letters A*, 119(2), 65–68.
25. Grebogi, C., Ott, E., & Yorke, J. A. (1983). Crises, sudden changes in chaotic attractors, and transient chaos. *Physica D-Nonlinear Phenomena*, 7(1–3), 181–200.
26. Pavlovskaja, E., & Wiercigroch, M. (2004). Analytical drift reconstruction for visco-elastic impact oscillators operating in periodic and chaotic regimes. *Chaos, Solitons and Fractals*, 19(1), 151–161.
27. Stefanski, A., & Kapitaniak, T. (2003). Estimation of the dominant Lyapunov exponent of non-smooth systems on the basis of maps synchronization. *Chaos Solitons and Fractals*, 15(2), 233–244.
28. Thompson, J. M. T., & Ghaffari, R. (1983). Chaotic dynamics of an impact oscillator. *Physical Review A*, 27(3), 1741–1743.
29. Thompson, J. M. T., & Stewart, H. B. (2002). *Nonlinear dynamics and chaos* (2nd ed.). Chichester: Wiley and Sons.



<http://www.springer.com/978-3-662-53092-4>

A Smooth and Discontinuous Oscillator

Theory, Methodology and Applications

Cao, Q.; Léger, A.

2017, XIX, 262 p. 131 illus., 54 illus. in color., Hardcover

ISBN: 978-3-662-53092-4